Wind-Electric Pump System Design

by

Edward Charles Lemmer

Submitted in partial fulfilment for the degree

Master of Science in Engineering

at

Stellenbosch University

Faculty of Engineering

Department of Electrical and Electronic Engineering

Supervisor: M.J Kamper

Date: March 2009

2.3.3 Estimating the Performance of a Wind-Electric Pumping System

The performance of a wind-electric pump system is defined as the volume of fluid delivered by the system in a given period of time, usually per annum. To estimate this system performance, the following must be known:

a)   Hydraulic output potential of the wind-electric pump system.

A wind-electric pump system can be designed to operate as efficiently as possible for an application with a certain pumping application and an available wind regime at the turbine installation site. The hydraulic output or pump delivery potential can be defined as the flow rate per hour that can potentially be achieved by the system at each wind speed that is presented to the turbine at the installation site. This hydraulic output potential can be approximated during the steady-state design of the system which will be discussed in Chapter 4. An example of such a WEPS hydraulic output potential is shown in Figure 5.
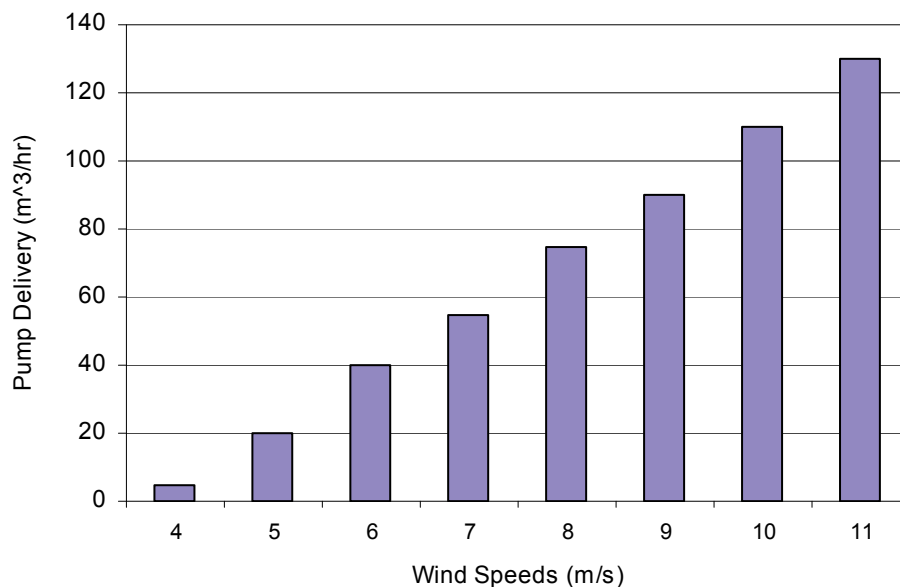

Figure 5: Example of a hydraulic output potential of a wind-electric system for each wind speed.

b)   The wind speed distribution at the site of the turbine application

It is a common error to use only the average wind speed at a turbine site to estimate the turbine performance. This method can underestimate or overestimate the actual performance of the turbine by up to 30 % according to Gipe [11]. By using the wind speed distribution of a site, more accurate performance estimations can be made because the contribution of each wind speed is taken into account. An example of such a wind speed distribution is given in Figure 6 in terms of the amount of hours that each wind speed would occur during the year. The contribution in pumped volume of each wind speed can be calculated as shown in Figure 7 by multiplying the estimated delivery potential of the wind-electric system for each wind speed in Figure 5 with the amount of hours of occurrence of each wind speed in Figure 6. The sum of these contributions is the per annum performance of the wind-electric system. The total per annum hydraulic output achieved by the wind-electric pump system performance in this example is therefore estimated from Figure 7 to be $\approx 358\ 000$ m³.
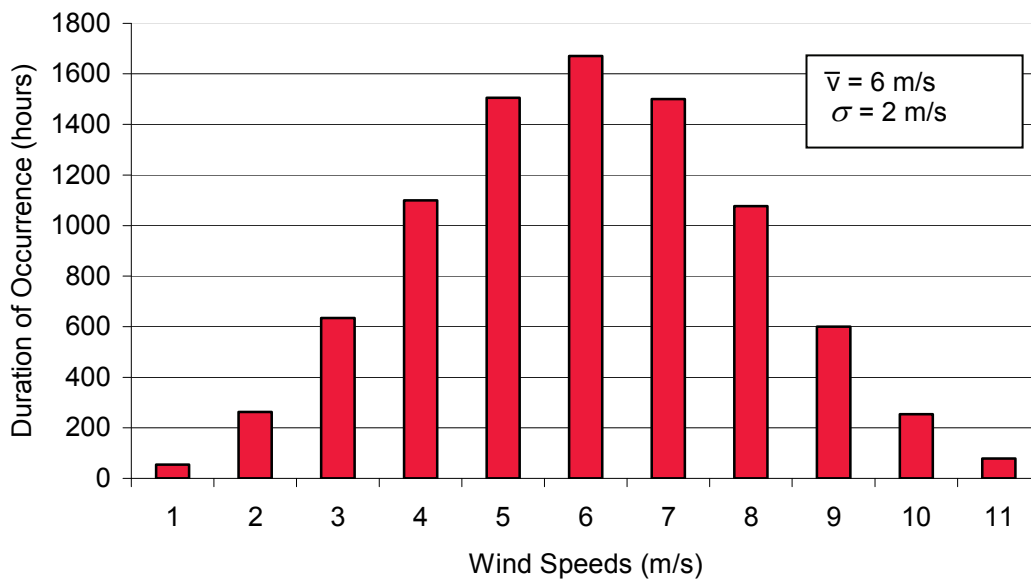

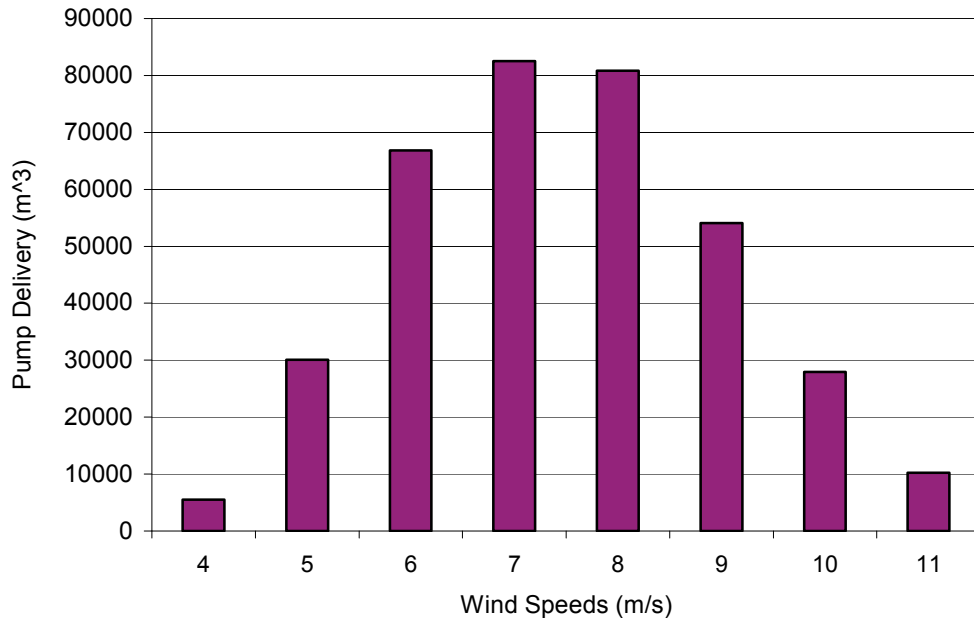**Figure 6: Example of a wind speed distribution.**

Figure 7: The contribution in pumped volume of each wind speed achieved by the wind-electric pump system.

where *K* is the sum of the nominal loss coefficients which depend on the type of pipe fittings, and *A* is the area of the circular pipe. The Hazen-Williams roughness coefficients, *C*, for different pipe materials and the nominal loss coefficients, *K*, for different pipe fittings are given in Sayers [22] – Hicks [28].
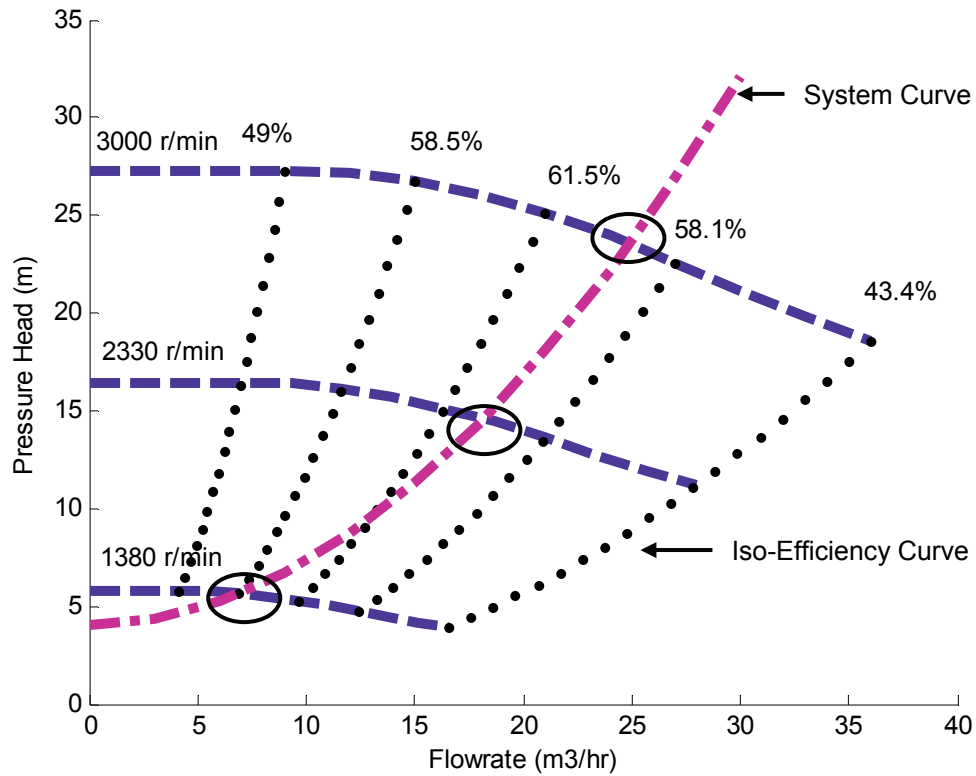

Figure 13: Example of pump performance curves at three different operating pump shaft speeds indicating pressure, flow rate and efficiency with a superimposed system curve.

are, however, ideally suited for implementation at boreholes where high pumping pressures are required. There are multi-stage pumps designed specifically for borehole applications. These specifically designed multi-stage borehole pumps have long cylindrical shapes which houses the numerous impellers. Specially designed induction motors of equal shape are incorporated with these borehole pumps to form long cylindrical units which are commercially available.

In the case of a parallel connection, the combined pump performance curve can be obtained by adding the different flow capacities of the parallel-connected pumps together at the same pressure heads. An example of this is also shown Figure 14 where two pumps with the same pump performance of P_1 and Q_1 at a given shaft speed are connected in parallel to form a combined performance of P_1 and Q_3. The only condition for parallel pumping is the fitment of non-return check valves on the discharge nozzles of each pump to prevent the discharge from one pump to reverse the flow through the other parallel-connected pump, causing potential damage to the pump impeller.
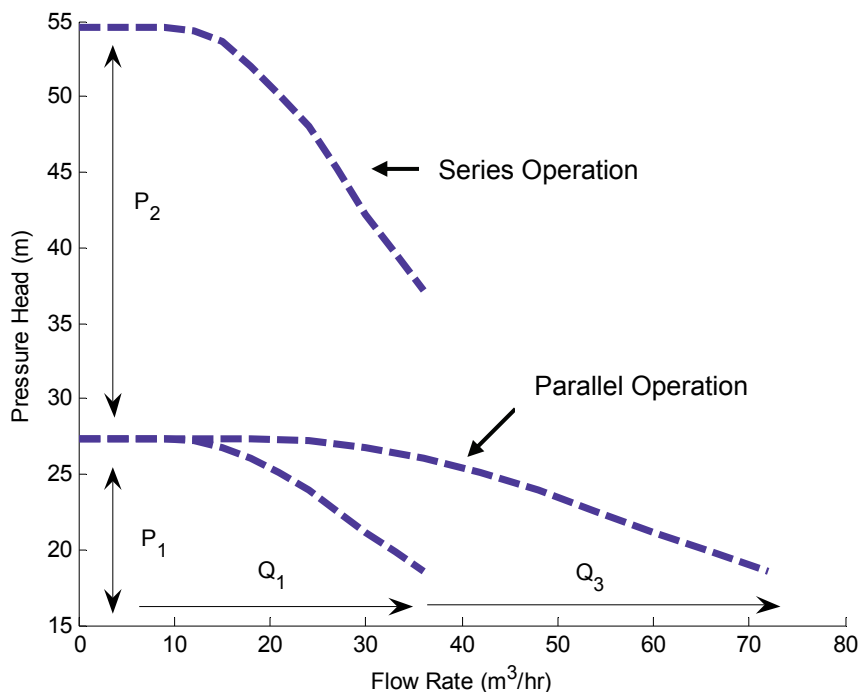

Figure 14: Example of the combined performance curves of two identical pumps connected in series and parallel. P_1, Q_1 is the pump performance curve of the pump indicated in Figure 13 at a shaft speed of 3000 r/min.

Because it is a low static head application, a low pressure, high flow pump was chosen. This chosen pump is the ETA-X 32-125 model manufactured by KSB Pumps. The pump performance curves of the pump are supplied by the pump manufacturer for shaft speeds of 2900 r/min for a 2-pole induction motor and 1450 r/ min for a 4-pole induction motor respectively. The pump performance curves are determined at other operating shaft speeds by using the pump affinity laws given by (3.59) - (3.60) which are shown in Figure 17.

The net positive suction head (NPSH$_R$) required by the pump to prevent cavitation, is provided by the pump manufacturer as varying between 0.4 m $-$ 1.3 m for flow rates between $0 - 40$ m³/hr. Stellenbosch is located at a height of 107 m above sea level which translates to $P_H \approx 100$ kPa. The temperature is assumed to be 20ºC which corresponds to a water vapour pressure of $P_{VP} \approx 2.34$ kPa. The suction pipe is directly connected from the tank outlet to the pump inlet with $H_{Ss} = 0$. The type of piping used is PVC with a pipe diameter of 40 mm. The suction pipe length is 0.5 m. The only pipe fitting in the suction line is a gate valve. The value of H_f can thus be calculated as being $H_f \approx 3.6$ m at the maximum flow rate of 40 m³/hr.
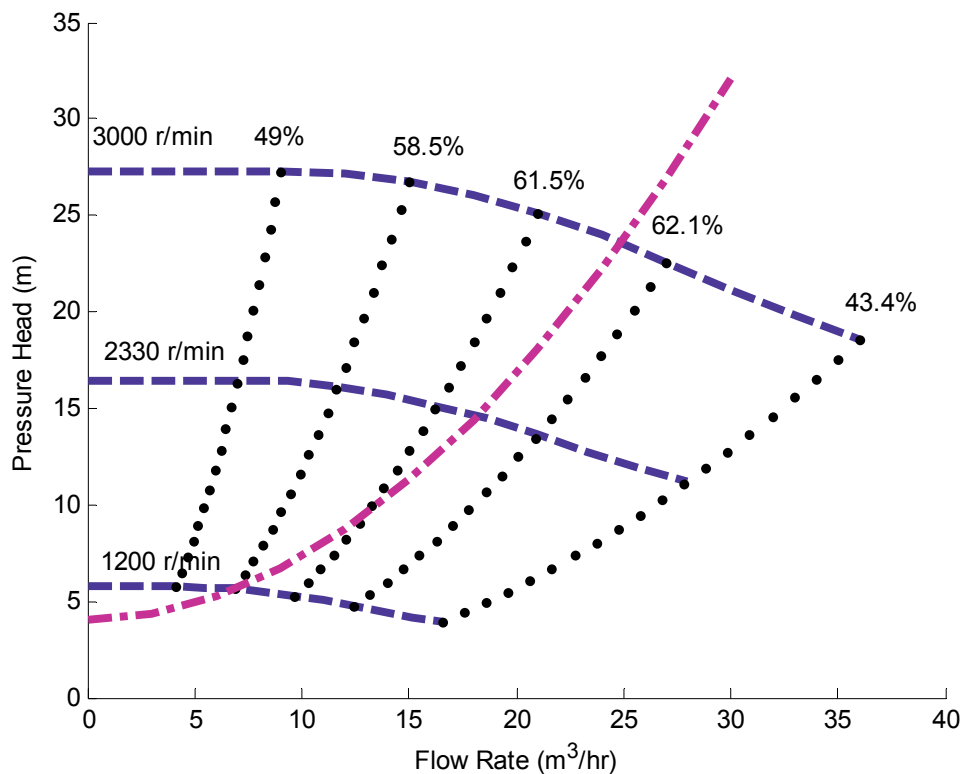

Figure 17: Pump performance curves of the KSB centrifugal pump model ETA-X 32-125 for different operating shaft speeds.

pump across its usable operating range are superimposed on Figure 18 using (4.6) for various shaft speed ratios. The value of motor slip in (4.6) is ignored at first to estimate the pole ratio required for good power matching. It can be seen from Figure 18 that a shaft speed ratio of 1:10 causes the pump to operate close to the optimum operation of the turbine and would provide good power matching between the turbine and the pump. A shaft speed ratio of 1:6 would, however, not provide as good a match. The steady-state operating turbine shaft speeds can, therefore, be estimated as between 125 r/min and 320 r/min for the 1:10 speed ratio. If a 4-pole induction motor is chosen, a 40-pole generator would have to be used which would generate a supply frequency of between 42 Hz and 106 Hz. If a 2-pole induction motor is used, a 20-pole generator would be needed which would generate a supply frequency of between 21 Hz and 53 Hz. The 4-pole induction motor is not a viable option in this application since the high frequency generated by the 40-pole generator would (i) cause unnecessarily high iron losses in the induction motor and (ii) reduce the bearing life since the induction motor would be operating at double its synchronous speed. In this application, the optimum power matching and utilisation of the turbine and pump is therefore achieved with the 1:10 speed ratio which, in turn, translates to a 20-pole generator and 2-pole induction motor.
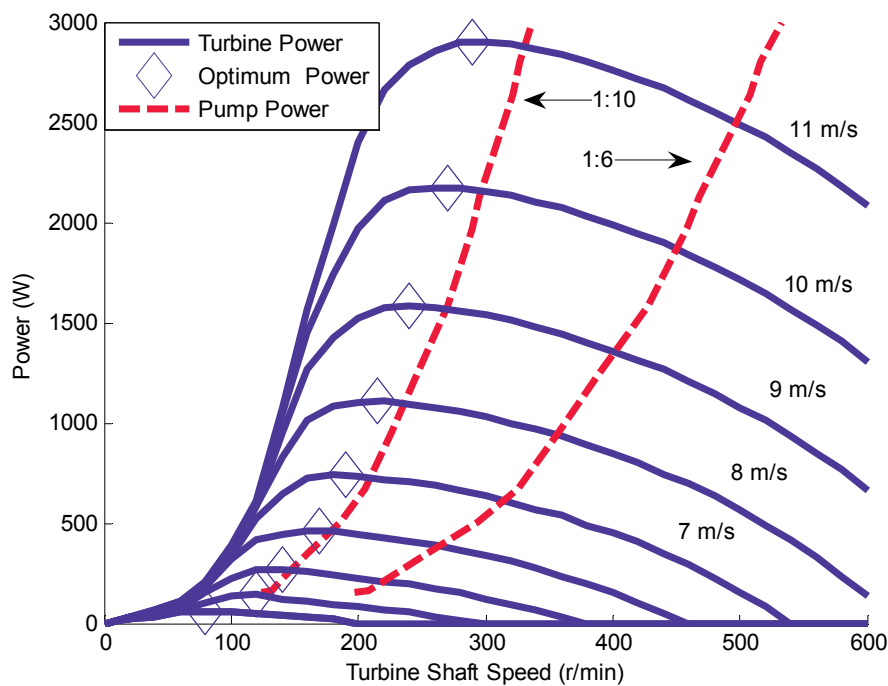

Figure 18: Estimated power flow between the 3 kW Aero Energy wind turbine and centrifugal pump for wind speed of 3 m/s – 11 m/s with shaft speed ratios of 1:10 and 1:6.

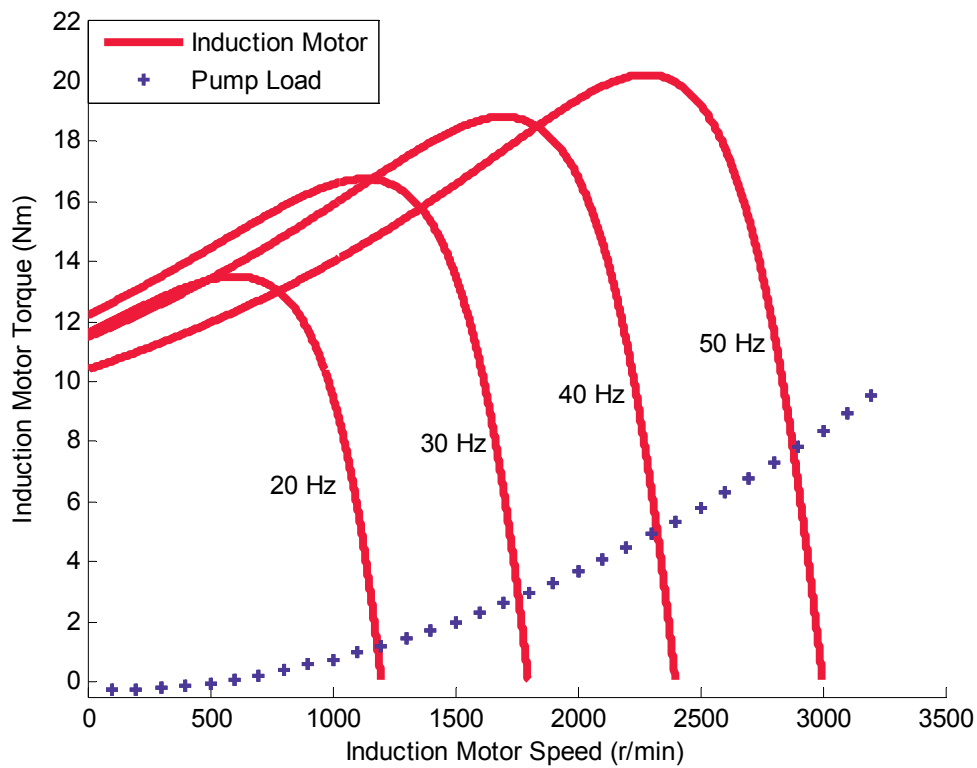| Performance Rating	2.2 kW @ 2850 r/min
Rated Voltage Supply	400 V, 3-Phase @ 50 Hz
Rated Efficiency	87.5 %
Rated Current	4.3 A
Number of Poles	2
Rated slip	5 %
Duty	0.86 PF
3-Phase Connection	Star
Insulation Class	F

Table 1: 2.2 kW Induction motor nameplate data

Figure 19: Calculated torque-speed curves of the 2.2 kW induction motor operating under constant V/Hz supply.
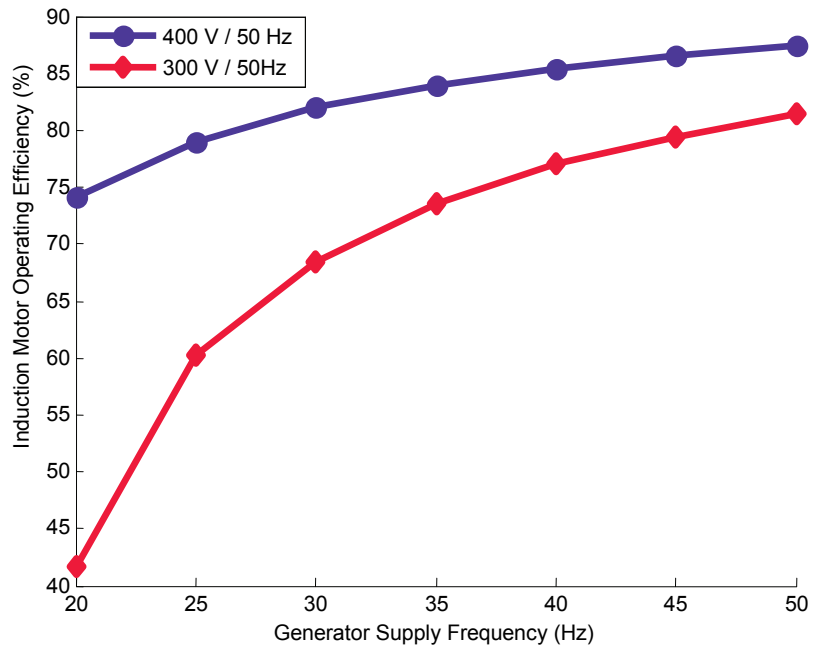
Figure 20: Operating efficiency of the 2.2 kW induction motor operating at 100 % of rated torque and supplied by a V/Hz supply ratio of 400 V/50 Hz and 300 V/50 Hz respectively.
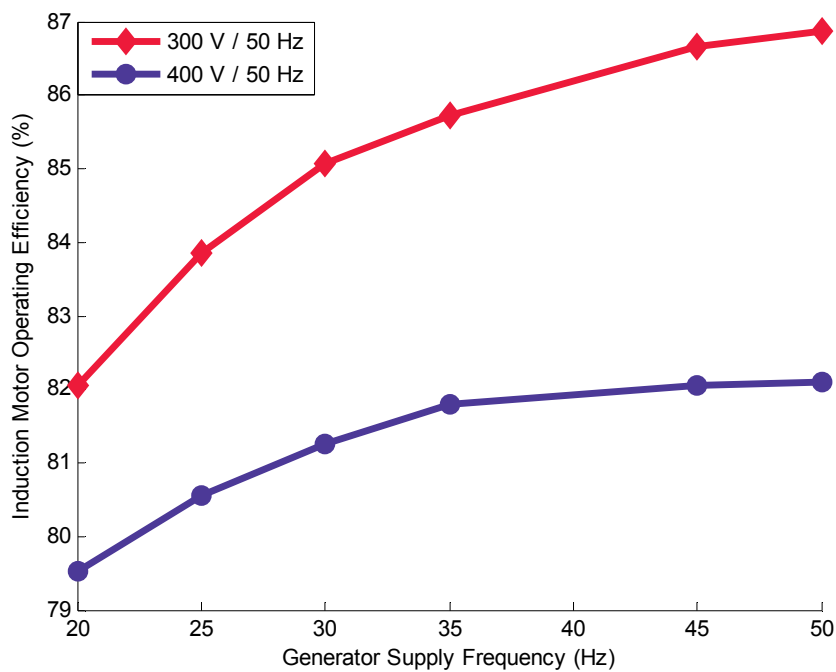

Figure 21: Operating efficiency of the 2.2 kW induction motor operating at 25 % of rated torque and supplied by a V/Hz supply ratio of 400 V/50 Hz and 300 V/50 Hz respectively.
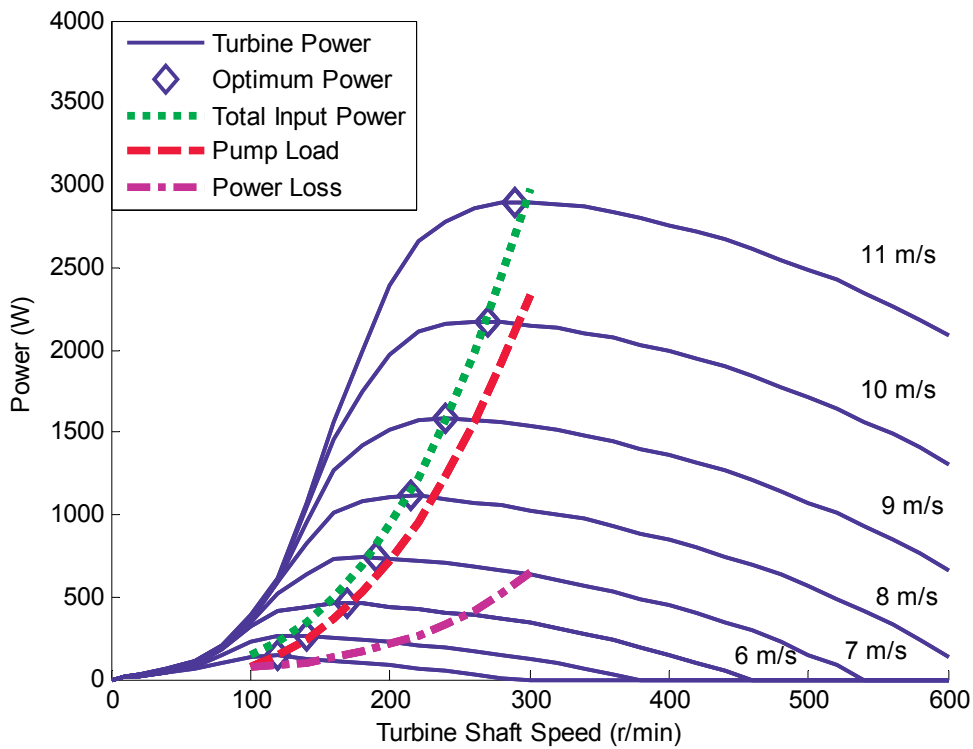
Figure 23: Total mechanical input power, pump load and electrical power loss of the wind-electric pump system depicted on the power delivery curves of the Aero Energy wind turbine for wind speeds of 4 m/s to 11 m/s.
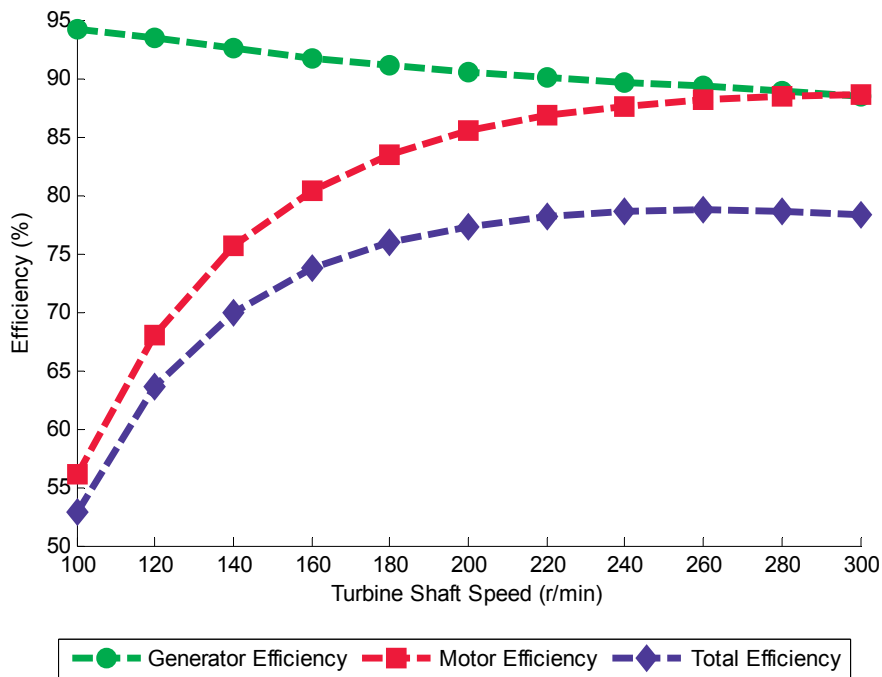

Figure 24: Calculated electrical efficiency of the permanent magnet generator and the induction motor across the operating range of the Aero Energy wind turbine.

4.6.2 Manufacture of Modified Stator

The stator coils were wound according to the specifications in Table 5 and placed in the 1 kW stator casting mould as shown in Figure 25. The stator coils were connected in wye as shown in Figure 22. The spaces between the coils were filled with fibreglass fibres which would bond with the epoxy to give structural integrity to the stator mould. The mould was then closed, filled with epoxy and baked overnight. The rotor and modified stator were then assembled and the complete generator assembly mounted on the test bench as shown in Figure 26.
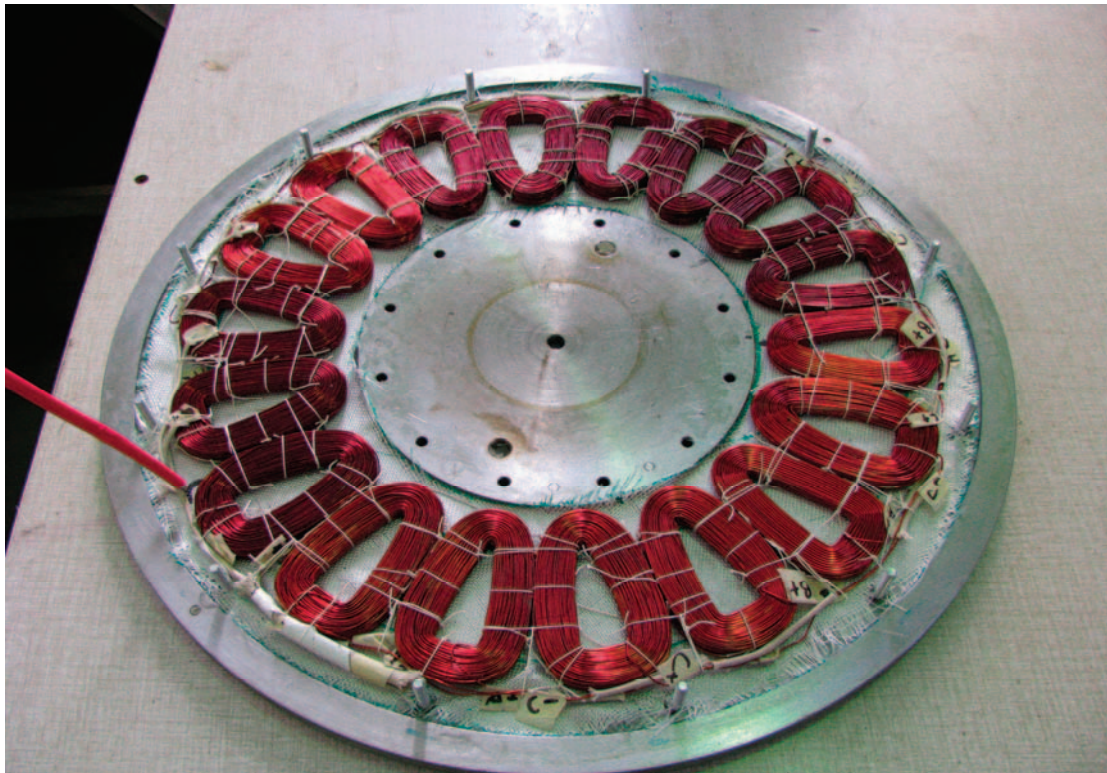

Figure 25: Stator coil layout in the casting mould before adding the epoxy.
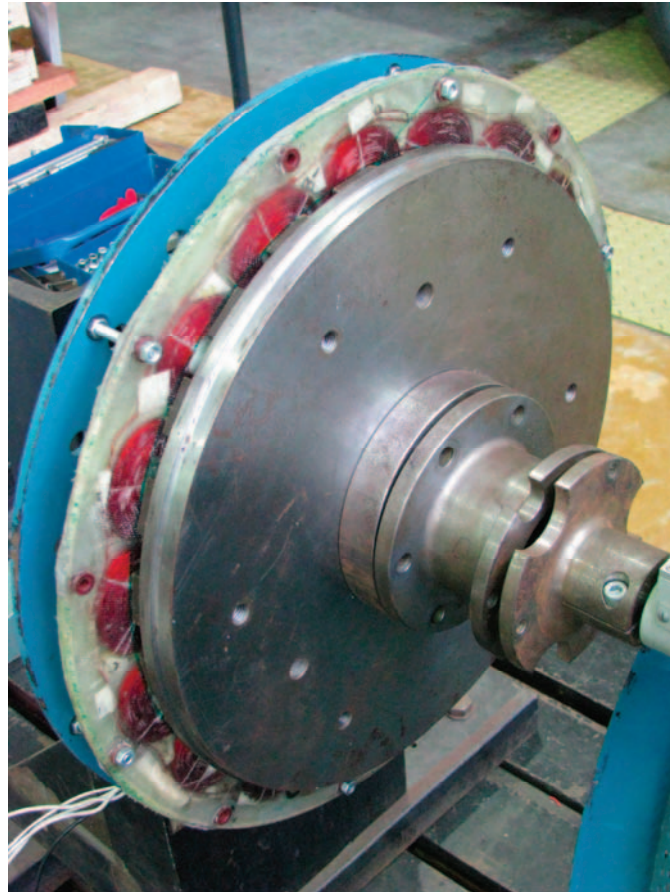
Figure 26: Complete generator assembly on the test bench.

4.6.3 Test Setup and Measuring Methodology

The steady-state operation of the system was tested in the laboratory using a test setup shown in Figure 27. The permanent magnet generator was driven at various shaft speed increments, Ω_1, using a 55 kW induction motor which is supplied by a variable speed drive. Torque and speed sensors were placed at both generator and motor shafts as shown in Figure 28 and Figure 29. These sensors allow the measurement of the mechanical input power supplied to the generator as well as the mechanical output power generated by the motor at each speed increment. The overall electrical operating efficiency for each speed increment could be determined through these measurements. The generator supply was also measured at each increment using a power analyser. The measured supply parameters include the generated electrical power, voltage, phase current and system power factor. A temperature probe was inserted in the stator mould to monitor the temperature of the windings, especially at high turbine shaft speeds. The generated water pressure in the pipeline was measured

using a pressure gauge. The induced water flow is measured by measuring the volume of water displaced from tank 1 to tank 2 in Figure 16 within a given amount of time. All the measurements made at each increment are listed in Appendix C.
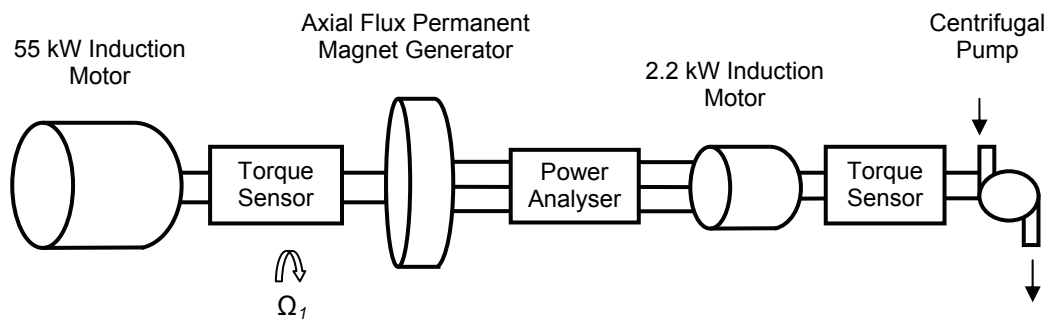

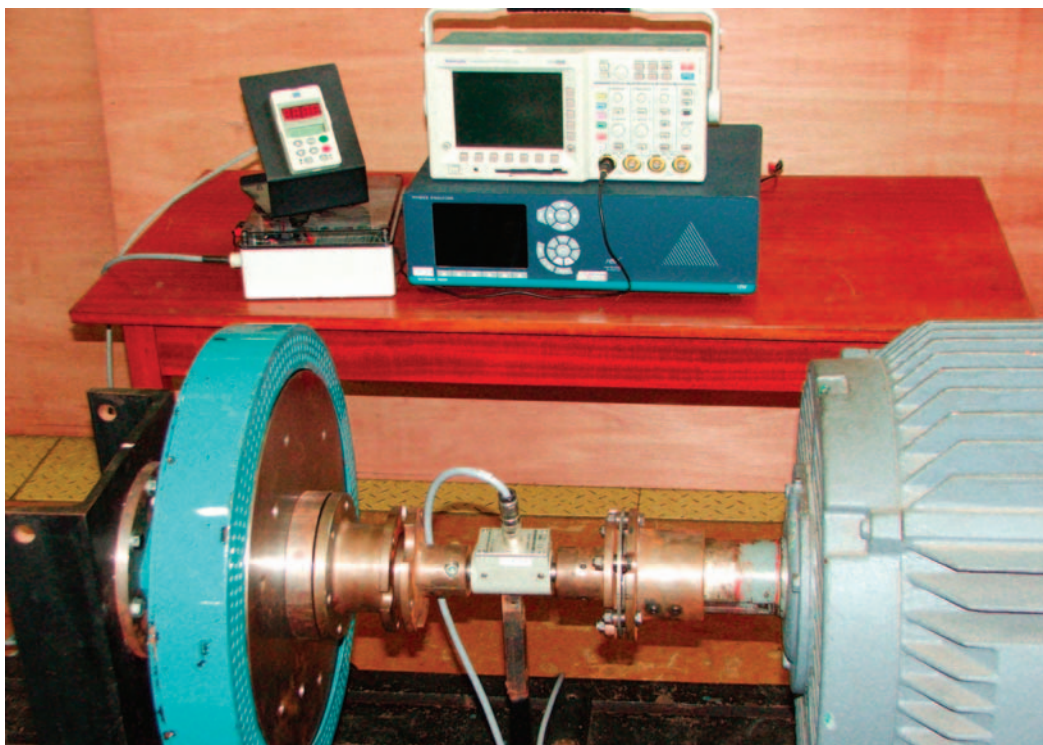**Figure 27: Block diagram of laboratory test setup.**

Figure 28: Test setup at the shaft between the assembled generator with the modified high voltage stator and the 55 kW induction motor. The torque sensor, power analyser and VSD control of the induction motor panel can be observed.

Figure 29: Test setup at the bottom tank of the re-circulating pump system. The torque and speed sensors at the shaft between the 2.2 kW induction motor and centrifugal pump can be observed.

4.6.4 Test Results

The total steady-state mechanical input power required to drive the wind-electric pump system is calculated across the operating range of the wind turbine based on the new set of permanent magnet generator design parameters given in Table 4 and Table 5 and shown in Figure 30. The 24 poles in the generator rotor mean that the wind-electric pump system, utilising the 2-pole motor, would have a shaft ratio of 1:12. The wind-electric pump system would therefore not operate as close to the optimum operation of the turbine as the 1:10 shaft ratio in Figure 23. The overall electrical operating efficiency of the generator and motor is also calculated across the operating range of the wind turbine and shown in Figure 31. The measurements made during the test setup are included in Figure 30 and Figure 31. The comparison between the calculated and measured steady-state operational data is shown in Figure 30 – Figure 31 to be accurate. This accurate steady-state operation comparison shows the system model derived in Chapter 3 and the calculation methodology in Appendix B to be accurate in estimating the steady-state operation of a wind-electric pump system.
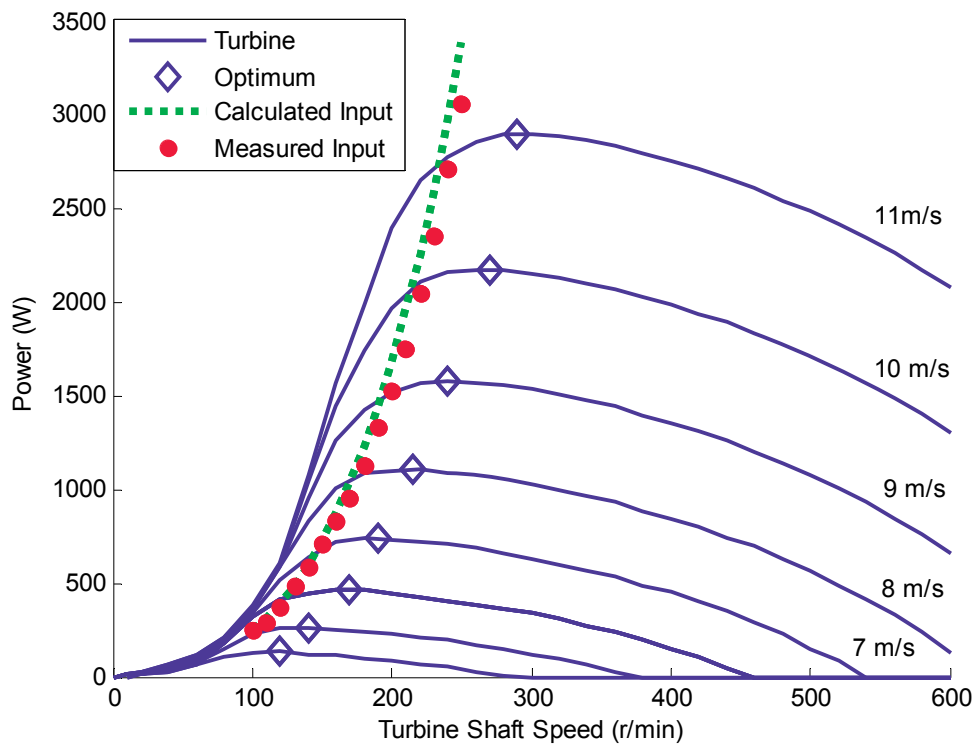
Figure 30: Calculated and measured total mechanical input power superimposed on the 3 kW turbine delivery curves for wind speeds of 4 m/s – 11 m/s.
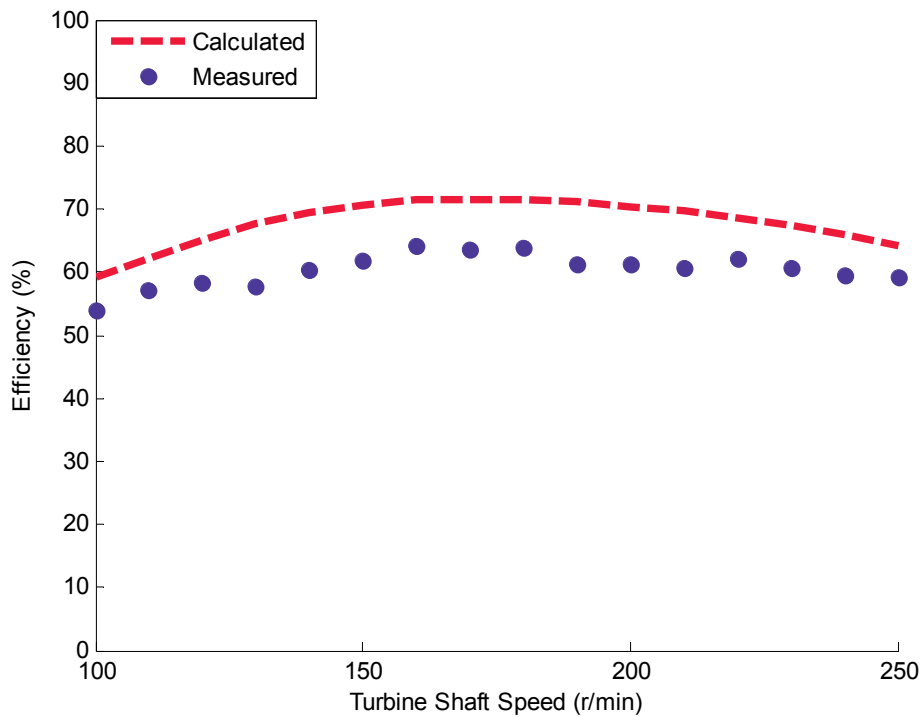

Figure 31: Calculated and measured combined efficiency of the permanent magnet generator and induction motor across the operating range of the wind turbine.

This accurate steady-state operation of the modified 1 kW generator design also serves to validate the design parameters and the steady-state operation of the original generator design discussed in Chapter 4.5.

The steady-state operation of the wind-electric pump system in Figure 30 is given in Table 6 for the maximum wind speed of 11 m/s. It can be deduced from the steady-state operating parameters in Table 6 that the limitations imposed on the modified high-voltage stator design resulted in the overloaded operation of the generator. The eddy current loss is very low due to the small diameter of the conductors used in the production of the modified stator, i.e. ≈ 0.8 mm but the high stator resistance caused a considerable voltage drop which increased the slip operation of the induction motor.

The generator and motor efficiency of the tested system are measured across the operating range of the wind turbine and shown in Figure 32. The motor efficiency improves, as expected, at higher generator shaft speed due to the increase in V/Hz terminal supply. The generator efficiency is high at low generator shaft speeds but drops substantially at higher generator shaft speeds due to the overloading of the generator.
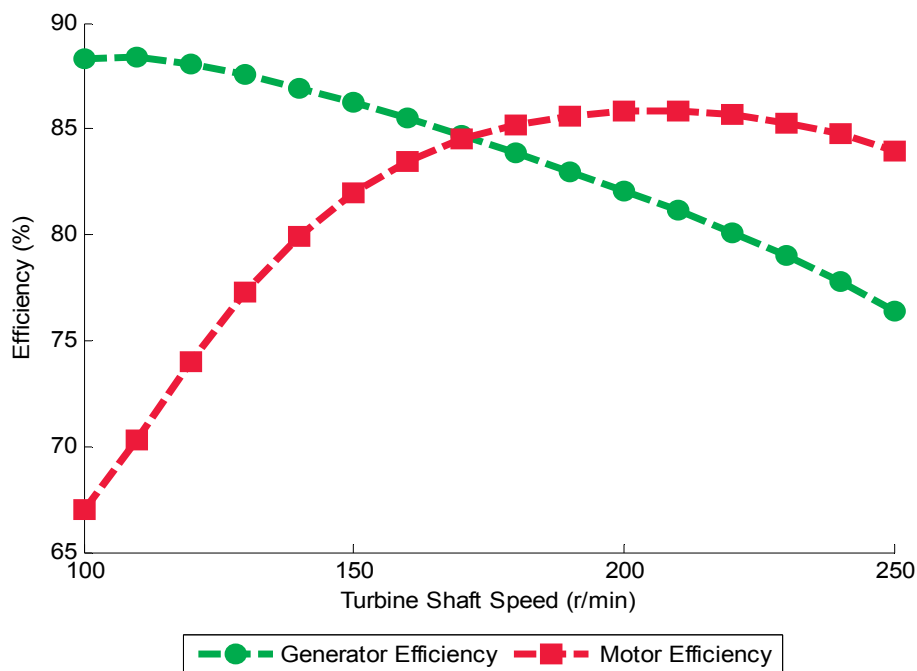

Figure 32: Measured electrical efficiency of the modified permanent magnet generator and the induction motor across the operating range of the Aero Energy wind turbine.

The current density in the stator conductors of the modified high-voltage stator is shown in Figure 33 throughout the operating range of the wind turbine. The current density at the maximum operating wind speed of 11 m/s is indicated in Figure 33 and calculated using (4.9) as being

$$J = \frac{(200)(4.87)}{(8.4)(21)(0.58)} \approx 9.8 \text{ A/mm}^2 . \tag{4.9}$$

It is therefore evident that the overloaded operation of the generator at 11 m/s wind speed caused the current density to be above the 6-7 A/mm² considered safe for the small air-cored stator. This extensive heat dissipation was also evident during testing. It is also shown in Figure 33 that the generator is operating within limits at a wind speed of about 9 m/s. The modified generator must therefore not be operated above a maximum wind speed of 9 m/s at a rating of 1.4 kW to ensure reliable and safe operation.
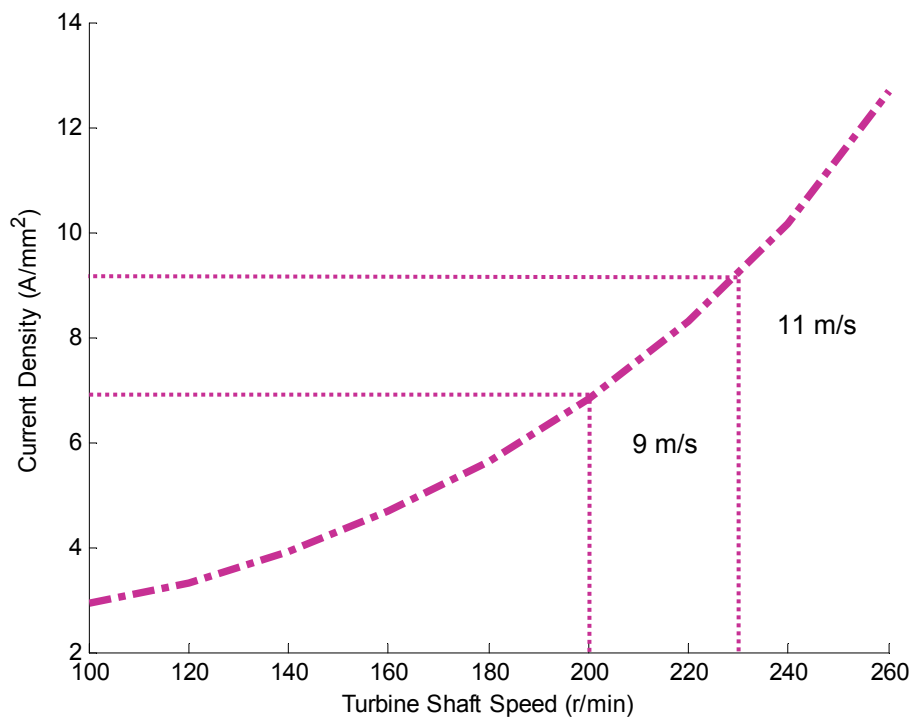

Figure 33: Current density in the conductors of the modified high voltage stator. The current density at the operating wind speeds of 9 m/s and 11 m/s are indicated.

The hydraulic delivery potential of the wind-electric system is measured and calculated at each wind speed and shown in Figure 34. The calculations are made using the steady-state operation of the WEPS shown in Figure 30 in conjunction with the performance curves of the ETA-X 32-125 pump shown in Figure 17. The copper losses caused by the high stator resistance of the permanent magnet stator mean that the tested wind-electric system can only start to operate at wind speeds above 5 m/s. This output potential can now be used in conjunction with a wind speed distribution at the turbine installation site to estimate the performance of the wind-electric pump system.
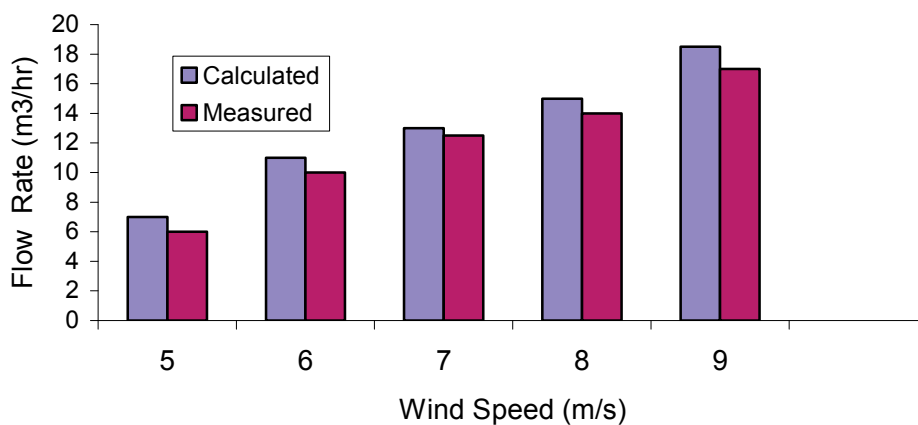

Figure 34: Estimated and measured hydraulic output potential of a wind-electric system for each wind speed.

4.6.5 Summary

An existing 1 kW axial flux permanent magnet generator design was modified and built for a high-voltage application. The generator was then analysed and tested to validate the system model of the wind-electric pump system derived in Chapter 3. The limitations imposed on the modified generator design reduced the generator rating. The operating range of both the wind turbine and centrifugal pump was therefore decreased which, in turn, decreased the hydraulic output potential of the wind-electric pump system. Chapter 4.5, however, shows that the performance of the wind-electric pump system can be much better if the guidelines given in the optimal design of the axial flux permanent magnet generator, are followed.
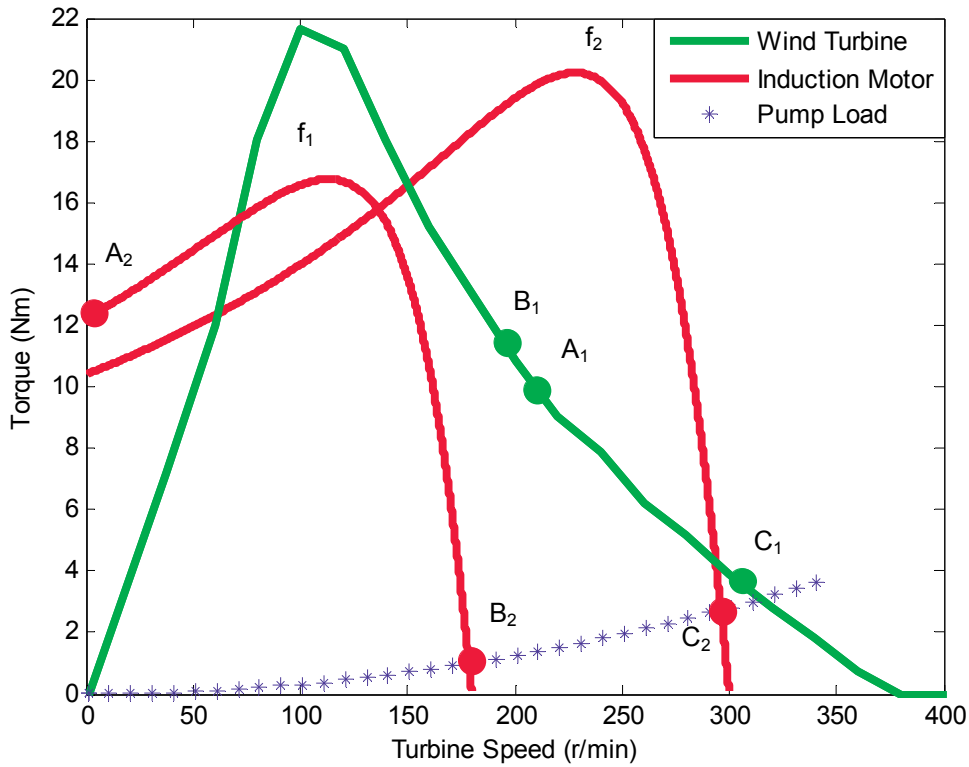
Figure 35: Torque characteristics of a wind turbine, induction motor and centrifugal pump used to illustrate the start-up process for a wind-electric pump system example.
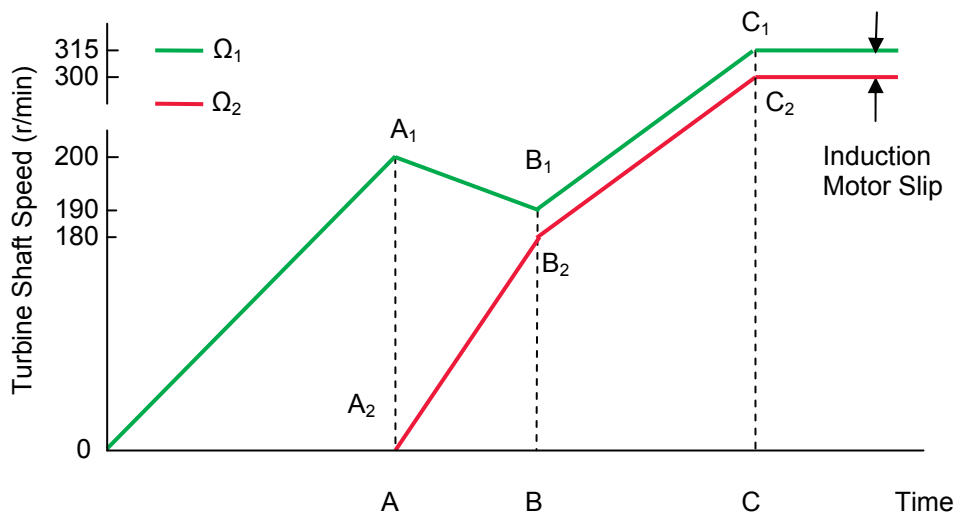

Figure 36: An example of the transient start-up behaviour of the wind-electric pump system example in Figure 35.
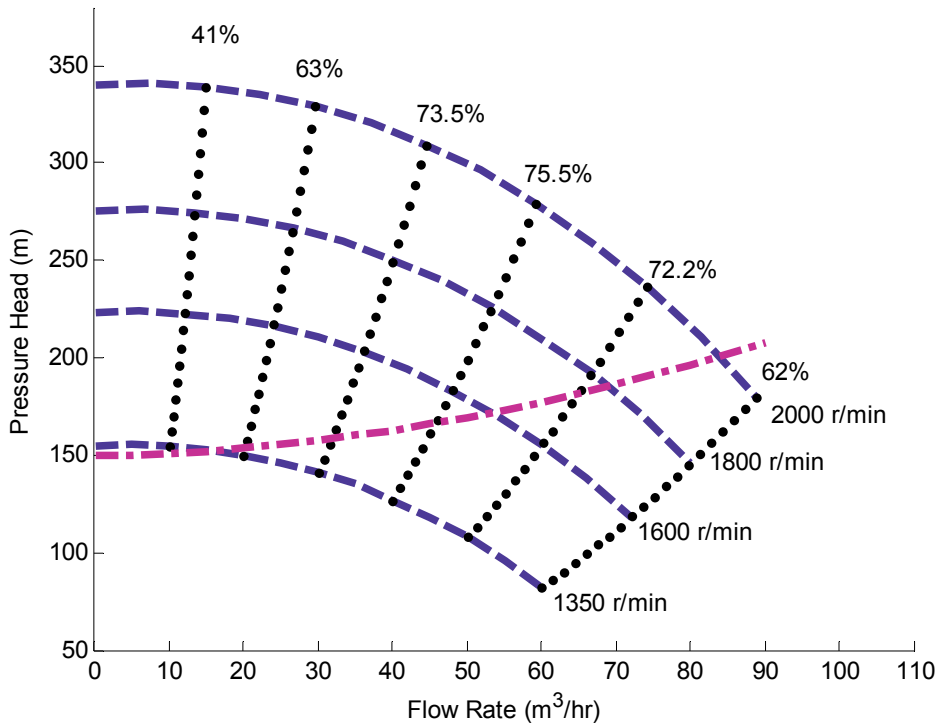
Figure 41: Pump performance curves of the KSB multi-stage centrifugal pump model MTC 65 6.1/11 for operating shaft speeds of 1350 r/min – 2000 r/min.

The larger pump that was chosen is the WKLN 80/4 model manufactured by KSB Pumps. The pump performance curves of this multi-stage pump are shown in Figure 42. The pump has four stages and could not be operated above 3500 r/min according to the operating manual. The required static head is generated at a shaft speed of ≈ 2100 r/min. The flow rate at the maximum efficiency of 74 % at the 2100 r/min operating speed is ≈ 80 m³/hr. The minimum flow rate required by the pump at this speed is estimated at ≈ 0.5 × 80 = 40 m³/hr. It can also be deduced from the intersection between the system curve and the 2100 r/min pump performance curve in Figure 42 that this minimum flow rate is achieved by the pump at this minimum operating shaft speed.
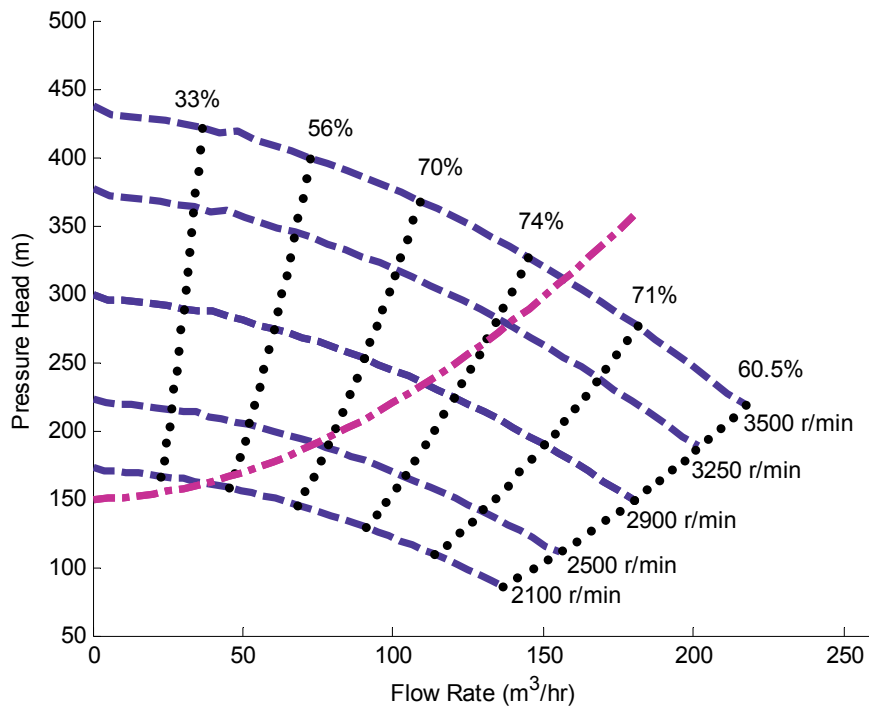
Figure 42: Pump performance curves of the KSB multi-stage centrifugal pump model WKLN 80/4 for operating shaft speeds of 2100 r/min – 3500 r/min.

6.4.3 Power Matching

The power delivery curves of the 323 kW wind turbine manufactured by Aero Energy is adjusted with the 0.9 factor and shown in Figure 43 for wind speeds of 3.5 m/s – 11.5 m/s. The power requirements of the two centrifugal pumps across their usable operating range are superimposed on the turbine power delivery curves using (4.6) for a shaft speed ratio of 1:60. The chosen shaft speed ratio would provide a good match between the wind turbine and the smaller pump under low wind speed conditions. The power matching between the wind turbine and larger pump during high wind speed conditions is within 95 % of the optimum turbine power. For 2-pole induction motors, a 120-pole generator would be needed which would generate a supply frequency of between 20 Hz and 60 Hz. From Figure 43 it is estimated that the large induction motor must have a rated performance of at least 185 kW and the smaller induction motor must have a rated performance of at least 70 kW. The induction motors were therefore rated at commercially available ratings of 200 kW and 75 kW respectively.
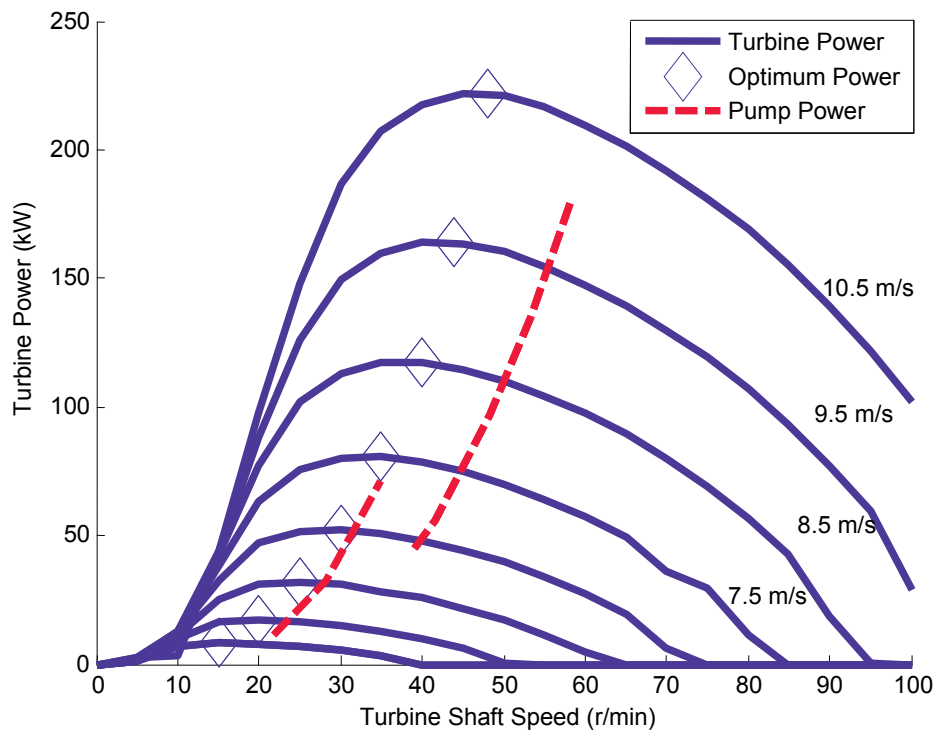
Figure 43: The power requirements of the two centrifugal pumps across their usable operating ranges are superimposed on the adjusted power delivery curves of the Aero Energy wind turbine for wind speeds of 3.5 m/s – 10.5 m/s utilising a shaft speed ratio of 1:60.

6.4.4 Design of Axial Flux Permanent Magnet Synchronous Generator

The design of the axial flux permanent magnet synchronous generator is optimised to operate at the maximum wind speed of 11.5 m/s at a minimum efficiency of 90 % without compromising the insulation properties of the stator epoxy through excessive current densities. The V/Hz supply of the generator is chosen to be 3000 kV/50 Hz. The large physical dimensions of this generator design mean that the air flow inside the air-cored stator would be more than in the small generator designs discussed in the previous chapters. The current density in the stator conductors can therefore be higher. The current density limit considered for the air-cored stator in this design is 10 A/mm².

The total number of coils in the 120-pole generator was chosen to be Qc = 90 in keeping with the desired coil pitch of θm = 4π/3. The axial thickness of the stator coils was chosen to be 20 mm. The peak flux density in the air-gap between the rotor-mounted magnets was also chosen as 0.6 T. Multiple parallel circuits i.e. a > 1 were used in this design to keep the diameter of the stator conductors to a minimum. This is
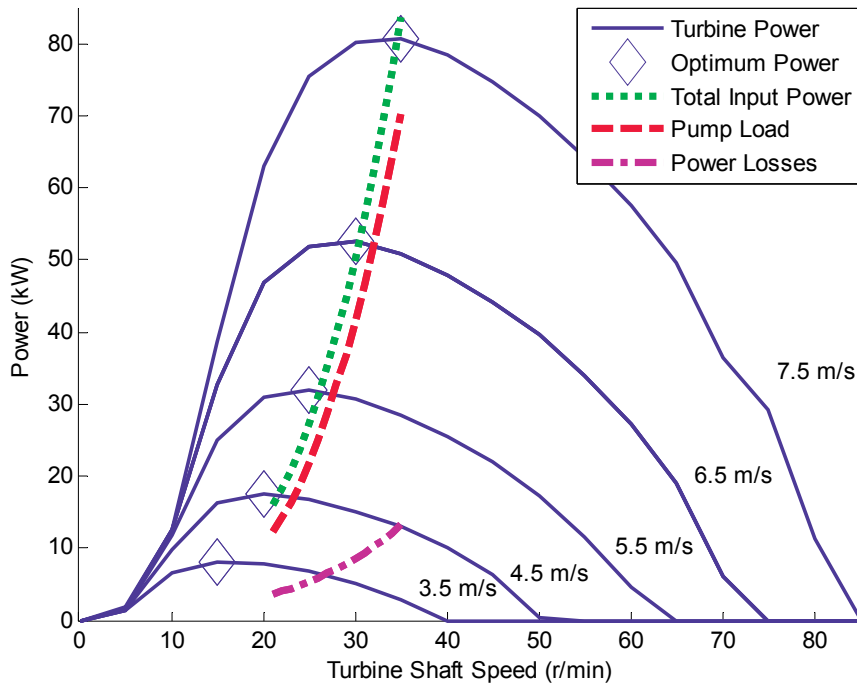
Figure 45: Total mechanical input power, smaller centrifugal pump load and electrical power loss of the wind-electric pump system depicted on the power delivery curves of the 300 kW Aero Energy wind turbine for wind speeds of 3.5 m/s to 7.5 m/s.
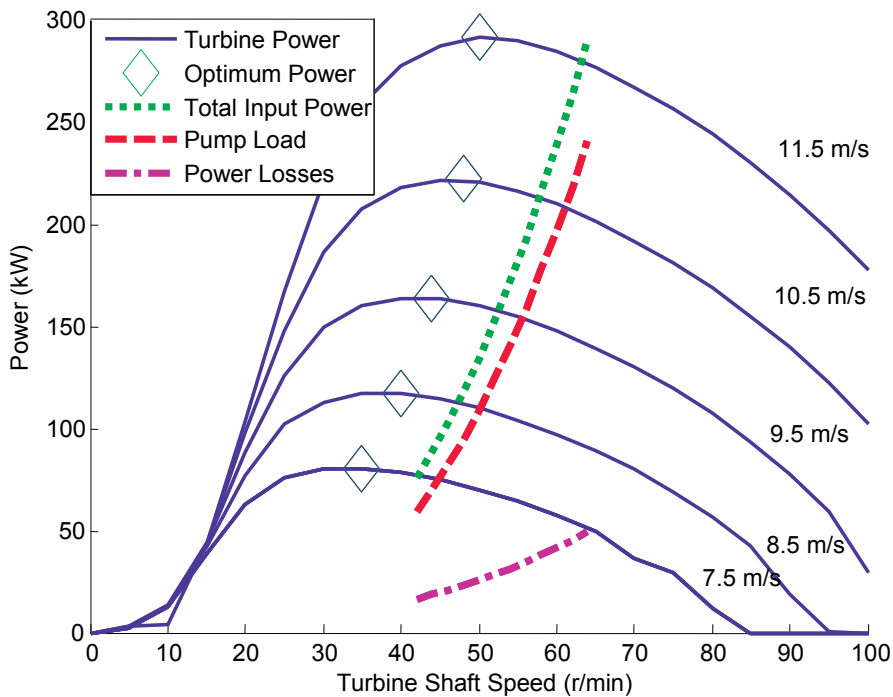

Figure 46: Total mechanical input power, larger centrifugal pump load and electrical power loss of the wind-electric pump system depicted on the power delivery curves of the 300 kW Aero Energy wind turbine for wind speeds of 7.5 m/s to 11.5 m/s.

The operating efficiencies of the WEPS that exist across the operating range of the wind turbine are calculated and shown in Figure 47 for the system using the smaller 75 kW induction motor and centrifugal pump and in Figure 48 for the system using the larger 200 kW induction motor and centrifugal pump. Large induction motors generally have high operating efficiencies due to their low slip operation which are reflected in the high operating efficiencies that are calculated for both induction motors across the operating range of the wind turbine. The generator design was optimised for the least internal stator impedance. The permanent magnet generator design could, however, not be optimised to operate at a minimum efficiency of 90 % throughout the operating range of the wind turbine. The is due to the eddy-current loss in the stator conductors which could not be reduced enough whilst still keeping within the stator conductor current density limit of 10 A/mm². The calculated current density in the stator conductors is shown in Figure 49 for the two separate motor-pump configurations. It is noted that the current density at the maximum wind speed of 11.5 m/s is close to the limit at ≈ 9.5 A/mm². The calculated operating efficiency of the permanent magnet generator throughout the operating range of the turbine is shown to be between 86 - 88 %. The transformer rating was calculated at the maximum considered operating wind speed of 11.5 m/s to be 250 kVA. The rating of the transformer was chosen with a safety factor to be 300 kVA as indicated in Figure 40.
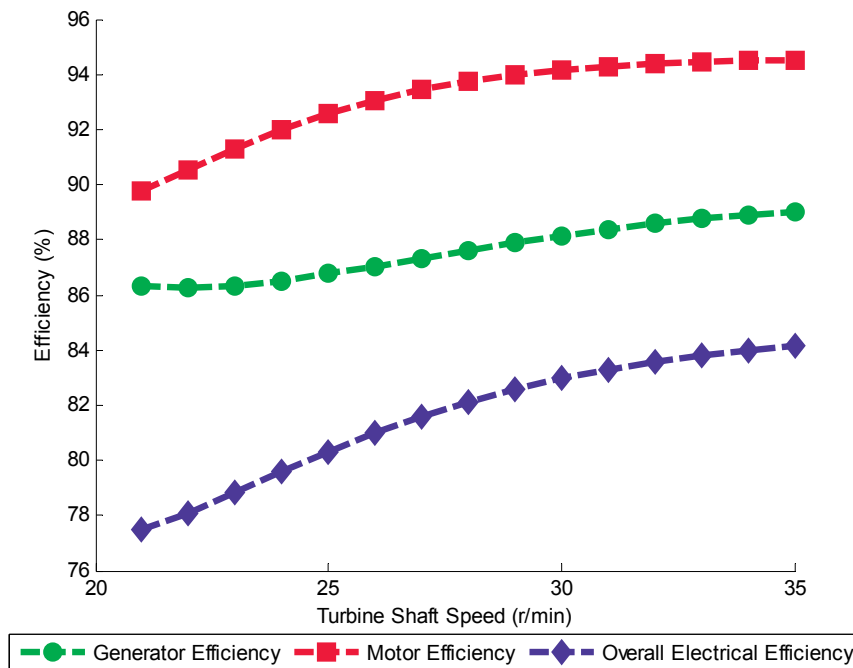

Figure 47: Calculated electrical efficiency of the permanent magnet generator and the 75 kW induction motor across the operating range of the Aero Energy wind turbine.
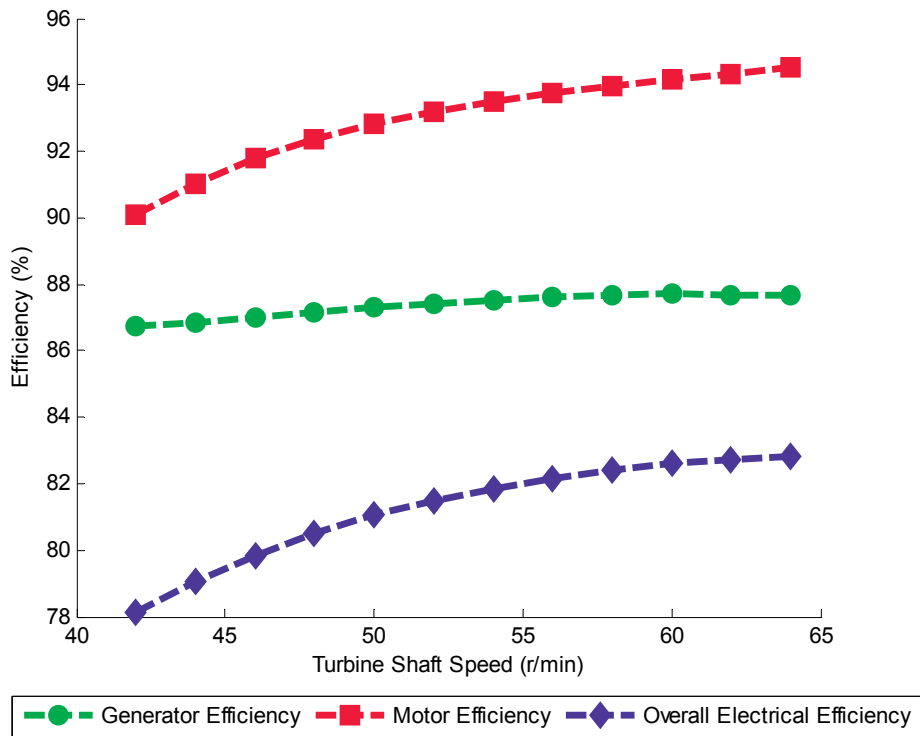
Figure 48: Calculated electrical efficiency of the permanent magnet generator and the 200 kW induction motor across the operating range of the Aero Energy wind turbine.
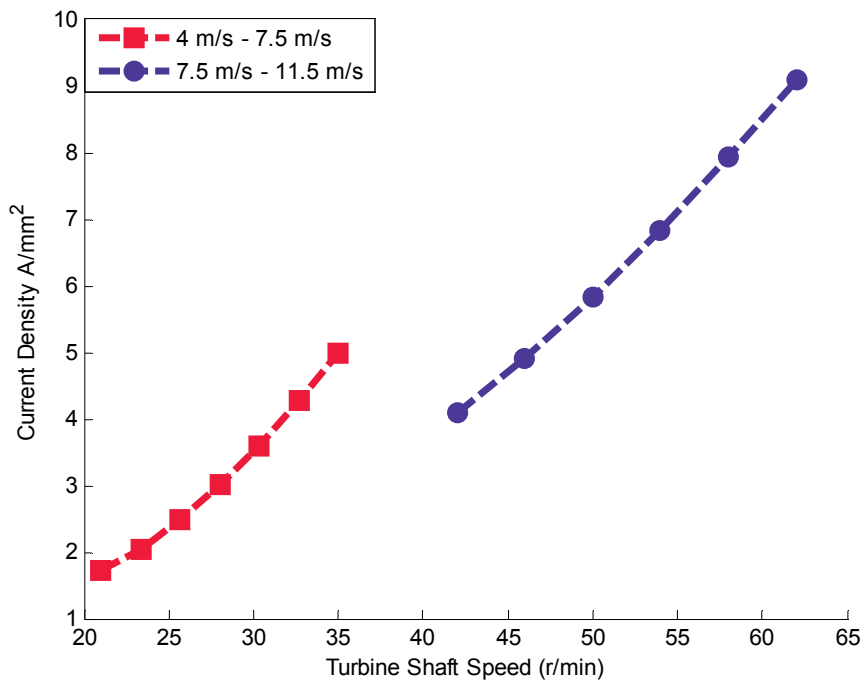

Figure 49: Calculated current density in the stator conductors for WEPS operation under the two separate wind speed ranges required by the two separate motor-pump configurations.

6.5   Wind-Electric Pump System Performance

The delivery potential of the wind-electric pump system at each wind speed is estimated based on the calculated steady-state operation of the WEPS and the pump performance curves of the two pumps and shown in Figure 50. Three possible annual wind speed distributions at the turbine installation site are shown in Figure 51. The average wind speed, $\bar{v}$, is changed for each of the three wind speeds with only the standard deviation, σ, remaining the same. The performance of the wind-electric pump system is estimated using the pump output potential in Figure 50 in conjunction with the different possible annual wind speed distributions in Figure 51. The total annual pumped output achieved by the wind-electric pump system performance is given in Table 8 for each of the different wind speed distribution scenarios. The additional continuous power that could be developed by the hydro-electric scheme due to the increased flow of the wind-electric pump scheme is also given. Note that this continuous developed power is only an average value based on the annual wind speed distributions. Seasonal variation in the wind speed distribution may alter the contribution of the wind-electric pump system to the flow rate that can be extracted from Boschberg Dam. The total increase in generation potential that the wind-electric pump system could contribute to the generation potential of the hydro-electric scheme is also given in Table 8 as a percentage value.
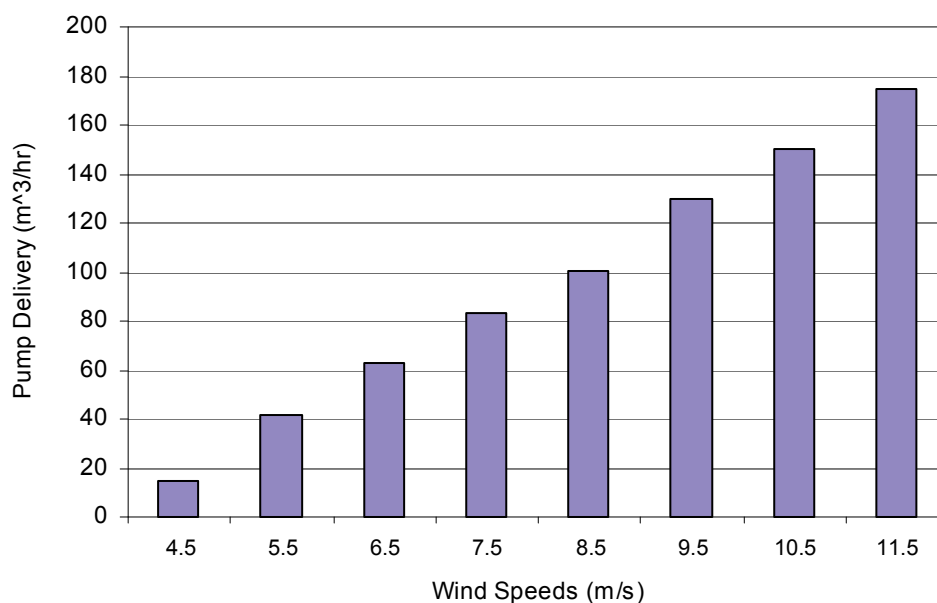

Figure 50: Example of the estimated wind-electric system delivery potential for each wind speed.

It can be seen that a high wind speed distribution with an average value of 8 m/s is necessary for the wind-electric pump system scheme to almost double the generation potential of the hydro-electric scheme.
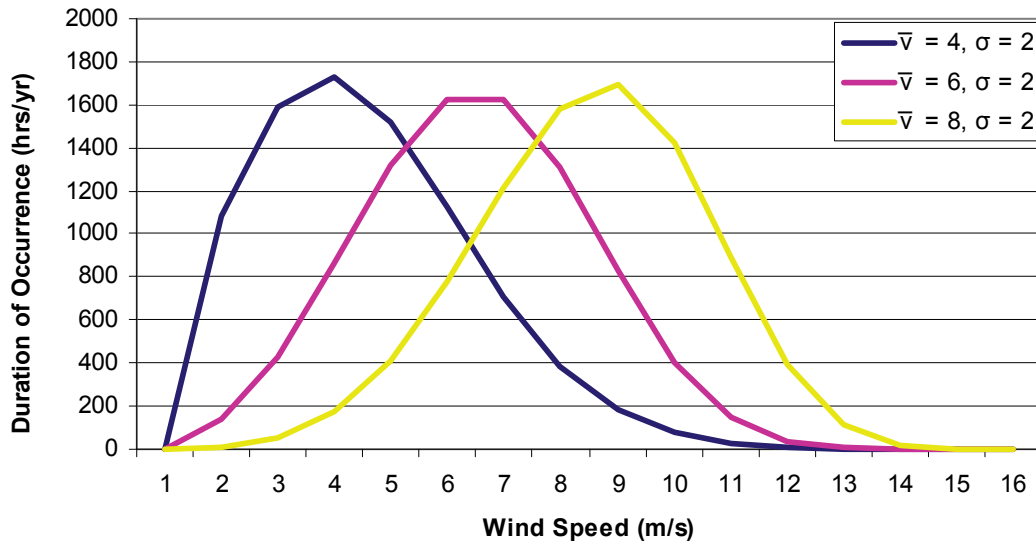

Figure 51: Annual wind speed distribution for different average wind speeds

Wind speed distribution	Total annual pumped volume output (m³)	Additional average continuous developed power (kW)	Increase in total generation potential of the hydro-electric scheme (%)
$\overline{v} = 4$, $\sigma = 2$	180 000	26	21
$\overline{v} = 6$, $\sigma = 2$	465 000	67	53
$\overline{v} = 8$, $\sigma = 2$	804 000	115	92

Table 8: Estimated generation potential of the wind-electric pump system installed at Boschberg mountain.

	From Measured Data:	From Manufacturer Data:
R_S	2.85 Ω (R_{LEAD} = 0.8 Ω)	2.8 Ω
R_R	2.5 Ω	2.9 Ω
X_S	4.13 Ω	4.8 Ω
X_R	4.13 Ω	4.8 Ω
X_M	132 Ω	122 Ω
R_{FE}	1600 Ω	1480 Ω

Table 11: Equivalent circuit parameters of the 2.2 kW induction motor derived from no-load and locked-rotor measurement data given in Table 10.
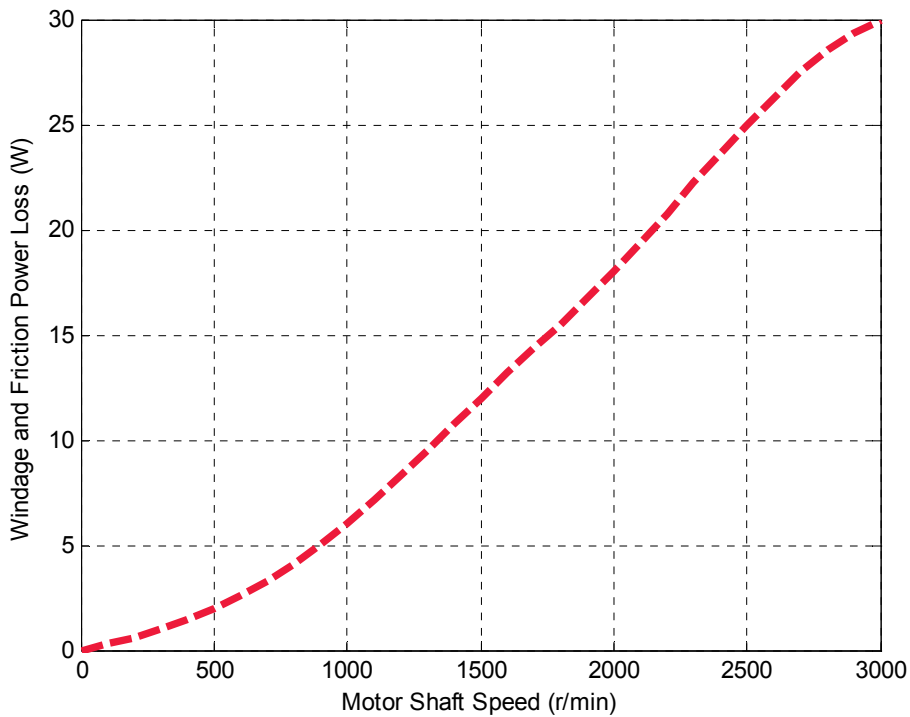

Figure 52: Windage and friction losses of the 2.2 kW induction motor versus various shaft speeds.